AGU PUBLICATIONS

Global Biogeochemical Cycles

RESEARCH ARTICLE
10.1002/2014GB004981

Key Points:
- New proxy to measure average settling velocities using ^{210}Po-^{210}Pb profiles
- Suggest clear shallow and mesopelagic contribution of slow-sinking particles
- Depth increase in velocities suggests slow particles remineralization up to 400 m

Supporting Information:
- Readme
- Figure S1a
- Figure S1b
- Figure S2
- Figure S3
- Figure S4
- Table S1
- Table S2

Correspondence to:
M. Villa-Alfageme,
mvilla@us.es

Citation:
Villa-Alfageme, M., F. de Soto, F. A. C. Le Moigne, S. L. C. Giering, R. Sanders, and R. García-Tenorio (2014), Observations and modeling of slow-sinking particles in the twilight zone, *Global Biogeochem. Cycles*, *28*, 1327–1342, doi:10.1002/2014GB004981.

Received 16 SEP 2014
Accepted 17 OCT 2014
Accepted article online 22 OCT 2014
Published online 28 NOV 2014

Observations and modeling of slow-sinking particles in the twilight zone

M. Villa-Alfageme[1], F. de Soto[2], F. A. C. Le Moigne[3], S. L. C. Giering[3,4], R. Sanders[3], and R. García-Tenorio[1]

[1]Departamento de Física Aplicada II, Universidad de Sevilla, Sevilla, Spain, [2]Departamento de Sistemas Físicos, Químicos y Naturales, Universidad Pablo de Olavide, Sevilla, Spain, [3]National Oceanography Centre, Southampton, UK, [4]Oceanlab, University of Aberdeen, Newburgh, UK

Abstract The biological carbon pump (BCP) transfers carbon from the surface ocean into the oceans' interior, mainly in the form of sinking particles with an organic component, and thereby keeps atmospheric CO_2 at significantly lower levels than if the oceans were abiotic. The depth at which these sinking particles are remineralized is a key control over atmospheric CO_2. Particle sinking speed is likely to be a critical parameter over remineralization depth. Carbon export is usually controlled by large, rapidly sinking particles ($>150\ m{\cdot}d^{-1}$); however, under some circumstances sinking velocity distributions are strongly bimodal with a significant fraction of total flux being carried by slowly ($<10\ m{\cdot}d^{-1}$) sinking particles. Therefore, there is an interest in determining sinking particle velocities and their variations with depth, as well as in understanding the interplay between sinking velocity distributions and carbon export. Here, we use profiles of total and particulate concentrations of the naturally occurring radionuclide pair ^{210}Po-^{210}Pb from the Porcupine Abyssal Plain (PAP) site (48°N, 16.5°W) to estimate depth variation in particle sinking speed using a one-box model and inverse techniques. Average sinking speeds increase from $60 \pm 30\ m{\cdot}d^{-1}$ at 50 m, to $75 \pm 25\ m{\cdot}d^{-1}$ and $90 \pm 20\ m{\cdot}d^{-1}$ at 150 and 500 m. Furthermore, a sensitivity analysis suggests that at the PAP site the measured ^{210}Po profiles are inconsistent with the usually assumed sinking velocities of $200\ m{\cdot}d^{-1}$. We hypothesize that a trend of increasing velocity with depth might be caused by a gradual loss of slow-sinking material with depth, a factor with significant implications for regional carbon budgets.

1. Introduction

The downward flux of particles from the surface ocean consists of a complex mix of biogeochemical material including particulate organic carbon (POC) and particulate inorganic "ballast" material such as opal, calcite, and lithogenic material. POC is of particular importance for organisms living in the dark ocean, as it is their main source of food. More than 90% of the POC exported from surface waters is respired to CO_2 by the biota in the "twilight zone" (the region between the euphotic zone and 1000 m depth) [e.g., *Robinson et al.* [2010]]. This respiration limits the depth to which particles are being exported, with only 0.01–3% of the POC produced in the surface waters being stored in deep-sea sediments, e.g., *Falkowski et al.* [1998].

The depth at which POC is respired is, according to models, an important control over atmospheric CO_2 levels [*Kwon et al.*, 2009; *De La Rocha*, 2003]. Yet, the mechanisms controlling this "remineralization depth" are unclear. Remineralization has been extensively studied in the last years (e.g., reviews by *De La Rocha and Passow* [2007], *Burd et al.* [2010], *Sanders et al.* [2014], and *Turner* [2014]) and is found to depend strongly on physical and geochemical factors as well as on the phytoplankton community in the site [*Buesseler et al.*, 2007; *Henson et al.*, 2012].

A factor likely involved in controlling remineralization depth is particle sinking speed. Slow-sinking particles ($<10\ m{\cdot}d^{-1}$) are more likely to be recycled at shallower depths, whereas fast-sinking particles are likely to reach greater depths before the organic carbon they contain is respired. The size and composition of sinking particles can change significantly due to repackaging by organisms resident in the oceans interior (e.g., *Lee et al.* [2009] and *Wilson et al.* [2008]), potentially leading to changes in sinking speed with depth. However, particle sinking speed is a difficult parameter to measure, and few studies have measured it.

Direct measurements have been done either in situ by using under-water cameras [*Sternberg et al.*, 1999] or after recovery in settling cylinders [*Alldredge and Gotschalk*, 1989; *Riley et al.*, 2012]. *McDonnell and Buesseler*

Table 1. Station ID, Sampling Time, and Position Taken for ^{210}Po/^{210}Pb During the D341

Station ID	Date	Latitude	Longitude
16477	13/07/2009	49.02°N	16.47°W
16497	16/07/2009	48.97°N	16.40°W
16523	20/07/2009	48.54°N	17.10°W
16544	23/07/2009	49.07°N	16.63°W
16583	29/07/2009	48.98°N	16.93°W
16592	31/07/2009	48.81°N	16.51°W
16619	03/08/2009	48.97°N	16.40°W
16640	06/08/2009	48.91°N	16.54°W
16659	08/08/2009	48.78°N	16.99°W

[2010] used in situ imaging of particles in viscous polyacrylamide gels to estimate the average sinking velocity of particles with equivalent spherical diameter between 45 μm and 10 mm as 10–150 m·d^{-1}. *Xue and Armstrong* [2009] developed a technique to determine settling velocities using the "benchmark" method, based on fitting Fourier series to time series data from sediment traps, which estimated sinking speeds of 220 ± 65 m·d^{-1} in the northwestern Mediterranean Sea.

Another direct technique used to estimate particle sinking speeds is the Indented Rotating Sphere (IRS) sediment trap [*Peterson et al.*, 2005, 1993; *Trull et al.*, 2008]. A recent synthesis of IRS results from a variety of settings [*Alonso-Gonzalez et al.*, 2010] suggests that two scenarios occur: either most POC flux is carried by very fast settling particles (velocities >300 m·d^{-1}), or the sinking speed distribution is bimodal with a significant fraction (up to 62%) of POC flux being associated with very slowly sinking material (<10 m·d^{-1}). However, aggregation of particles on the sphere prior to rotation may alter particle characteristics and reduce their sinking speeds [*Peterson et al.*, 2009]. Sinking speeds diagnosed from IRS traps therefore need to be confirmed by alternative methodologies [*Trull et al.*, 2008], such as locating cameras above and below the IRS [*Peterson et al.*, 2009].

Here we use an alternative method to track particle flux and sinking velocity: the disequilibrium between polonium-210 and its parent lead-210 (the ^{210}Po-^{210}Pb pair) [*Le Moigne et al.*, 2013b]. This approach is analogous to the widely applied ^{234}Th-method [*Stewart et al.*, 2010; *Verdeny et al.*, 2009] but has the advantage that the longer half-life of ^{210}Po (138 days vs 24 days for ^{234}Th) allows the disequilibria to penetrate deeper into the twilight zone compared to the ^{234}Th disequilibria [*Le Moigne et al.*, 2013b]. Furthermore, ^{210}Po is not only adsorbed to particles, but also assimilated by some phytoplankton and bacteria [*Fisher et al.*, 1983] and substitutes for S in proteins [*Stewart et al.*, 2007a]. Due to this strong biological affinity ^{210}Po is expected to trace POC export effectively.

In this paper, we use the observed profiles of ^{210}Po and ^{210}Pb to calculate particle-settling speeds throughout the water column. A one-box model with multiple vertical layers is built and fitted to ^{210}Po and ^{210}Pb profiles from the Porcupine Abyssal Plain (PAP) site (48°N, 16.5°W) in July 2009 [*Le Moigne et al.*, 2013b] to diagnose sinking velocity. Our calculations are validated by applying the same methodology to the ^{234}Th-^{238}U profiles measured in the PAP site in order to obtain alternative particle-settling speeds as well as by comparison to measurements made using the Marine Snow Catcher [*Riley et al.*, 2012]. Finally, the limitations of the approach are analyzed. We discuss the potential contribution of slow-sinking particles (<10 m·d^{-1}) to the downward flux as well as the dependence of this flux with depth and its penetration into the twilight zone.

2. Methods

2.1. Sample Collection

Samples for the analysis of ^{210}Po and ^{210}Pb were collected in July/August 2009 at 10 stations at the PAP site (Table 1) during cruise D341 onboard R.R.S *Discovery*. The PAP site is located on the boundary between the subpolar and subtropical gyres of the North Atlantic [*Henson et al.*, 2009]. Water was collected using a 24-bottle stainless steel sampling rosette equipped with 20-L Niskin® bottles, a CTD sensor, and a fluorimeter.

For total ^{210}Po and ^{210}Pb analysis, samples were taken at 10–15 depths from 5 to ~1000 m, with the highest resolution in the top 150 m of the water column. Five-liter samples were collected at each depth in acid- and MilliQ-cleaned carboys that were acid cleaned and pre-rinsed with the sample. Duplicate samples were taken at three different depths over the cruise, to check the reproducibility of the procedure.

Reproducibility was within the uncertainty of the measurements (~8% for ^{210}Pb and ~13% for ^{210}Po) with average values being 9% for ^{210}Pb and 15% for ^{210}Po.

Total ^{210}Po and ^{210}Pb analyses followed the GEOTRACES protocol [*GEOTRACES Standards and Intercalibration Committee*, 2010; *Rigaud et al.*, 2013] which involves scavenging using $Fe(OH)_3$ followed by ^{210}Po self-deposition onto a silver disk to give uncorrected ^{210}Po activity. ^{209}Po and stable lead were added as yield tracers. Additional plating was performed to remove any traces of Po and to ensure that only ^{210}Pb remained in solution with less than 5% of ^{209}Po being found on the second plating disk. A second ^{209}Po spike was added at this point to monitor recovery after Po ingrowth. Since some of the initial ^{209}Po tracer could have remained in the solution, this possibility was tested, and less than 5% of the initial tracer was found in the cleaning disk. Nevertheless, to eliminate overestimation of the radiochemical yield in the measurement of ^{210}Pb, when the solution was ^{209}Po-spiked a second time the amount was an order of magnitude higher than the amount added on board. Samples were stored to allow ^{210}Po in-growth via ^{210}Pb decay to occur. After at least 6 months, ^{210}Po and ^{209}Po were plated, and ^{210}Po activity was measured. ^{210}Pb activity was inferred from the second ^{210}Po analysis after the appropriate decay corrections were applied. Recoveries for Pb were obtained by ICP-MS measurement. Once ^{210}Pb had been determined, the initial measurement of ^{210}Po had to be corrected due to the decay of ^{210}Pb into additional ^{210}Po prior to ^{210}Po-^{210}Pb separations. ^{210}Po measurements were also decay corrected from the measurement to plating, as well as from plating to sampling. ^{210}Bi and ^{210}Po in-growth were both considered in the ^{210}Pb decay corrections. Contamination due to ^{210}Pb-^{210}Po present in the lead carrier was subtracted. The activity of the internal tracer ^{209}Po was decay corrected from the reference date to the measurement date. Counting was undertaken using a PIPS-type alpha detector (Canberra) at CITIUS (Centro de Investigación, Tecnología e Innovación, Universidad de Sevilla), with a full background correction. Uncertainties were obtained by error propagation.

Particles were collected by filtering large volumes (1000–2500 L) of seawater using in situ pumps (Stand Alone Pumping Systems—SAPS, Challenger Oceanic ®) through 53 and 1 μm pore size nylon mesh. The particles were rinsed off the meshes and split using a Folsom Splitter. Subsamples of the 53 (large) and 1 μm (small) fractions were filtered onto glass fibre filters (GF/F 0.7 μm pore size, Whatman) for subsequent ^{210}Po and ^{210}Pb analysis. Filters were fully digested in a mix of HNO_3, hydrochloric acid, and hydrofluoric acids. After evaporation, samples were redissolved in concentrated hydrochloric acid and then analyzed following the procedure documented above for water samples. Additional details of the radiochemical pre-treatment for water and particles can be found in *Le Moigne et al.* [2013b].

2.2. Model Development

A variety of approaches have been used to model, analyze, and interpret the observed activity of thorium in seawater [*Savoye et al.*, 2006]. Explicit modeling of thorium geochemistry has been used to simulate thorium distributions and thus to diagnose fluxes, as well as to model, simulate, and test sampling strategies [*Burd et al.*, 2000; *Resplandy et al.*, 2012]. In contrast, inverse modeling techniques use the comparison between model results and existing data to tune model parameter values until model results give the best agreement with the data. *Marchal and Lam* [2012], *Murnane and Cochran* [1991], and *Murnane et al.* [1994, 1996] developed inverse techniques in a three-box export model to obtain rate constants describing thorium and particle cycling in the ocean.

Efforts to understand ^{210}Po particle dynamics via modeling are relatively rare. We focus here on a simple export model of ^{210}Po that combines particulate and dissolved polonium into a single box, based on the equations used to calculate ^{234}Th or ^{210}Po fluxes [*Buesseler et al.*, 2001; *Verdeny et al.*, 2009]. The model explicitly incorporates particle-sinking speed as an unknown. Potential sinking speeds are derived by an inverse modeling approach that fits the observed profiles to the model whilst assuming steady state conditions. The systematic uncertainty of the latter assumption will be examined.

We assume that time variation in ^{210}Po activity $(a_{^{210}Po})$ at a given depth z is due entirely to the radioactive decay of ^{210}Po, the decay of ^{210}Pb into ^{210}Po, and the sinking of particles which carry ^{210}Po to the next depth,

$$\frac{da_{^{210}Po}(t)}{dt} = \lambda_{^{210}Po}(a_{^{210}Pb} - a_{^{210}Po}) + \frac{dP_{^{210}Po}(z,t)}{dz} \quad (1)$$

where $a_{210_{Pb}}(z)$ and $a_{210_{Po}}(z)$ are, respectively, ^{210}Pb and ^{210}Po total specific activities (e.g., in dpm·100 L^{-1}), $\lambda_{210_{Po}}$ is the ^{210}Po decay constant (0.005 d^{-1}), and $P_{210_{Po}}$ is downward ^{210}Po flux.

The simplest case of steady state conditions is assumed, where there is no time variation in activities or ^{210}Po flux over the half life of ^{210}Po (138 days). Thus, the total activity of ^{210}Pb and its daughter ^{210}Po can only differ from each other due to a downward flux of ^{210}Po, with the extent of this downward flux governing the size of the offset. The key point is that this assumption allows ^{210}Po flux to be written in terms of ^{210}Po activity in particles and their average bulk sinking speed $v(z)$

$$P_{210Po}(z,t) = a_{210Po}^{particle}(z) \cdot v(z) = a_{210Po} \frac{a_{210Po}^{particle}(z)}{a_{210Po}} \cdot v(z) = a_{210Po} \cdot f(z) \cdot v(z) \tag{2}$$

where $f(z)$ is the fraction of ^{210}Po in particles:

$$f(z) = \frac{a_{210Po}^{particle}(z)}{a_{210Po}} \tag{3}$$

$a_{210Po}^{particle}$ is the ^{210}Po measured in particles, comprising the sum of the small (1–53 μm) and large (>53 μm) fractions. a_{210Po} is the total ^{210}Po measured in seawater, including both particulate and dissolved ^{210}Po. Combining and rearranging equations (1) and (2) allows the size of the ^{210}Po-^{210}Pb disequilibrium (and hence the downward ^{210}Po flux) to be expressed in terms of sinking speed (equation (4)).

$$a_{210Pb} - a_{210Po} = -\frac{1}{\lambda_{210Po}} \frac{d(a_{210Po} \cdot (z) \cdot v(z) \cdot f(z))}{dz} \tag{4}$$

This equation is traditionally used in the literature to calculate ^{234}Th and ^{210}Po fluxes [*Buesseler et al.*, 2001; *Cochran and Masque*, 2003; *Savoye et al.*, 2006; *Verdeny et al.*, 2009]; here it is written in terms of speed, allowing us to obtain particle sinking speed throughout the water column.

Rearranging equation (4) allows ^{210}Pb and ^{210}Po activities to be related to $\delta(z)$ which has dimensions of depth (in m) and which will be used to calculate sinking velocities:

$$\delta(z) = \frac{f(z) \cdot v(z)}{\lambda_{210_{Po}}} \tag{5}$$

The traditional approach involves computing the downward Po flux using equation (1) and measured ^{210}Po and ^{210}Pb activities and $\delta(z)$ is not explicitly calculated. One of the aims of this work is to check the ability of equation (1) to describe real ^{210}Po profiles. Thus, inverse techniques are used here, and Po flux is not calculated. Instead, ^{210}Po activity is estimated, leaving $\delta(z)$ the only parameter to be tuned. To solve equation (4) ^{210}Po activity will be obtained from tuning the parameter $\delta(z)$ and from direct field measurements of $a_{210_{Pb}}(z)$.

2.3. Inverse Method

This section describes how ^{210}Po is estimated from observed ^{210}Pb specific activities using an inverse model. First, since our measurements are at discrete depths the finite difference is substituted for the derivative. Equation (4) is thus transformed into equation (6)

$$a_{210Pb} - a_{210Po} = -\frac{1}{h} \cdot \frac{(a_{210Po} \cdot (z+h) \cdot f(z+h) \cdot v(z+h)) - (a_{210Po} \cdot (z) \cdot f(z) \cdot v(z))}{\lambda_{210Po}} \tag{6}$$

where h is the depth between sampling points. Equation (6) allows us to calculate theoretical ^{210}Po specific activity from observed ^{210}Pb specific activity through the water column.

Equation (7) is obtained by writing equation (6) in terms of $\delta(x)$.

$$a_{210Po}^{MODELLED}(z) = a_{210Pb}^{MEASURED}(z) + \frac{\delta(z+h) \cdot a_{210Po}^{MODELLED}(z+h) - \delta(z) \cdot a_{210Po}^{MODELLED}(z)}{h} \tag{7}$$

Finally, modeled ^{210}Po at the next depth is calculated by solving the previous equation as follows:

$$a_{210Po}^{MODELLED}(z+h) = \frac{1}{\delta(z+h)} \left(\delta(z) \cdot a_{210Po}^{MODELLED}(z) - h \cdot \left(a_{210Pb}^{MEASURED}(z) - a_{210Po}^{MODELLED}(z)\right)\right) \tag{8}$$

Equation (8) can be used to estimate ^{210}Po at any depth $(z+h)$ from the measured ^{210}Pb activity at the previous depth, z, using modeled ^{210}Po activity calculated at z. The solution of the differential equation, either numerically or analytically, requires choosing an initial condition $a_{210}Po(z_0)$ at some

depth. The initial value of ^{210}Po is, in most cases, chosen to be the value measured at the shallowest sampled depth, $a_{^{210}Po}^{MEASURED}(z_0)$.

We tune the value of δ(z) and fit the model to measured ^{210}Po specific activity using a simplified least squares method to minimize the reduced chi squared, χ^2_{red}, defined as:

$$\chi^2_{red} = \frac{1}{n}\sum\left(\frac{a_{Po}^{MOD}(z) - a_{Po}^{EXP}(z)}{\Delta a_{Po}^{EXP}(z)}\right)^2 \quad (9)$$

where n is the number of degrees of freedom.

2.4. ^{210}Po Deficit as a Proxy to Calculate Sinking Speed

The tuning of $\delta(z)$ reveals potential changes in particle sinking speed with depth, which will be explored in subsequent sections. The average particle sinking speed at a given depth is obtained by evaluating $v(z)$ using equations (3), (5), and (6);

$$v(z) = \frac{\delta(z)\cdot\lambda_{^{210}Po}\cdot a_{^{210}Po}(z)}{a_{^{210}Po}^{particle}(z)} = \frac{\delta(z)\cdot\lambda_{^{210}Po}}{f(z)} \quad (10)$$

where $\lambda_{^{210}Po}$ is the decay constant (0.005 d^{-1}). It follows that particle sinking speeds at a particular depth can be calculated if the fraction of ^{210}Po in particles ($f(z)$), the decay constant, and $\delta(z)$ are known. $\delta(z)$ was taken as the value that produced the best fit between model and observations (see above). $f(z)$ was calculated from total ^{210}Po measured in the water samples and the particles collected from the in situ pumps (calculated as the sum of the two particle-size classes, 1–53 μm and >53 μm) (Table 3).

3. Results

3.1. Biogeochemical and Physical Conditions at PAP Site

At the Porcupine Abyssal Plain (PAP) site the annually integrated primary productivity is ~200 g C·m^{-2}·yr^{-1} [*Lampitt et al.*, 2010]. During cruise D341 (Figures S1a and S1b), chlorophyll-a concentrations derived from satellite data (MODIS) displayed two peaks prior to the cruise, one in mid-May (0.9 mg chl-a m^{-3}) followed by a second peak in mid-June (0.6 mg chl-a·m^{-3}). Primary productivity calculated from satellite data (PP) presented a typical pattern of increasing PP over the productive season reaching a peak in late June (2000 mg C·m^{-2}·d^{-1}) [*Le Moigne et al.*, 2013b]. PIC concentrations showed a peak in mid May (6×10^{-4} mol·m^{-3}), which matched the Chl-a trend. The depth of the mixed layer (MLD) in winter is typically ~350 m at this site [*Steinhoff et al.*, 2010]. That summer mixed layer depth (MLD) ranged between 31 (St. 16640) and 62 m (St. 16659), averaging 44 ± 11 m (determined by temperature difference, see temperature and salinity plots, Figure S2).

The T-S diagrams (Figure S3) show that there is a distinct mixed layer. The water mass between MLD and ~600 m at all stations was East North Atlantic Central Water of polar origin (ENACWp), though some influence of the Mediterranean Overflow Water (MOW) could be seen below 600 m [*Hartman et al.,* 2010].

The phytoplankton community was composed of a mixture of silicifying and calcifying phytoplankton [*Le Moigne et al.*, 2013b]. During D341 cruise *Riley et al.* [2012] collected 459 particles containing organic matter using a marine snow catcher. Two categories were observed, Marine Snow Aggregates (MSA, 429 particles) and particles consisting of a distinct solid centre of biomineralizing protist enveloped in marine snow (APC, 30 particles). The sinking speed of the fast pool was calculated as a weighted average of the MSA (180 ± 22 m·d^{-1}) and the APC (232 ± 58 m·d^{-1}). The average sinking speed of the slow settling fraction was estimated by *Riley et al.* [2012] to be 9 m·d^{-1}. Previous cruises at the site revealed that the microplankton (5–200 μm) community in the area comprised diatoms, dinoflagellates, planktonic ciliates and nanoflagellates [*Smythe-Wright et al.*, 2010], and radiolarians [*Lampitt et al.*, 2009].

Deep sediment traps at the PAP site have shown strong regional and seasonal variations in downward particle flux at depths from 1000 to 4700 m [*Lampitt et al.*, 2009], and very large pulses of particulate organic matter intermittently sink into the deep waters of the open ocean in the Northeast Atlantic. These variations have been attributed to changes in upper-ocean biogeochemistry and phytoplankton community [*Lampitt et al.*, 2009] and to spatial-temporal variability in surface waters [*Smythe-Wright et al.*, 2010].

3.2. ^{210}Po-^{210}Pb Profiles

The minima in total ^{210}Po activity lay between 50 and 100 m depth and ranged from 2.7 to 6.6 dpm·100 L^{-1} with an average value of 4.6 ± 2.0 dpm·100 L^{-1} (Figure 1 and Table S1 in Supplementary material). The maxima in ^{210}Po specific activity were found at the surface (5–25 m) and in the mesopelagic zone (below 800 m) and ranged from 5.5 to 12.6 dpm·100 L^{-1} with an average value of 7.6 ± 2.0 dpm·100 L^{-1}.

^{210}Po activities were lower than ^{210}Pb at every depth due to Po accumulation and adsorption onto sinking particles [*Le Moigne et al.*, 2013b]. Profiles of ^{210}Po and ^{210}Pb specific activities showed the greatest disequilibrium between 50 and 150 m, and indicated higher particle export rates in these regions. Below 500 m ^{210}Po activities slowly increased whereas ^{210}Pb activities decreased, with equilibrium being rarely found above 1000 m.

Table 3 shows measured particulate ^{210}Po activity at different depths and the associated values of *f(z)* calculated using equation (3). A weak dependence of both particulate ^{210}Po and the ratio of particulate to total ^{210}Po activity (*f(z)*) with depth is observed. Particulate ^{210}Po reached a minimum at 150 m in most stations with average *f(z)* being largest at 50 m, closest to the MLD.

3.3. Model Fit

$\delta(z)$ was evaluated by tuning the model to fit the direct field measurements of ^{210}Po activities ($a_{^{210}\mathrm{Po}}(z_0)$), using Pearson's chi-squared test (χ^2_{red}), defined in equation (9).

Initially, we assumed that $\delta(z)$ is constant through the water column (0–1000 m depth). The best solution for $\delta(z)$ ($\delta = 1100$ m), described ^{210}Po specific activities at depth well, but failed to reproduce the ^{210}Po specific activities at shallower depths (0 – ~50 m). This behavior indicates that $\frac{a^{particle}_{^{210}Po}}{a_{^{210}Po}} \cdot v(z)$ is depth dependent and allows us therefore to abandon the concept of a constant $\delta(z)$ throughout the entire water column.

$\delta(z)$ is the product of the fraction $f(z)$ of ^{210}Po activity in particles and the velocity $v(z)$ of settling particles, a change of $\delta(z)$ with depth can therefore be caused by changes in either f or v with depth. Our data show a local extremum indicating a change in the slope of ^{210}Po and ^{210}Pb specific activity profiles at around 50 m (see Figure 1). In ^{210}Po this is a minimum in specific activity indicating where the maximum ^{210}Po export occurs. This maximum in turn signals the depth of maximum particle export and roughly coincides with the MLD in most cases (Figures 1 and S2), although the resolution of our profiles does not allow us to discern if this maximum export is above or below the MLD.

We therefore adopted a *two-stage* $\delta(z)$ approach, with δ_0 as the value of δ between the surface and some intermediate depth (h), and δ_h as the value of δ between h and greater depths. This intermediate depth, h, was chosen for each profile individually, at the point where the vertical ^{210}Po gradient changed (Figure 1) indicating the local minimum in ^{210}Po concentration. We then calculated ^{210}Po activity depth by depth using measured ^{210}Pb values and the measured value of ^{210}Po at the shallowest depth as a boundary condition. For each profile, values for δ_0 and δ_h values (shown in Table 2) were chosen to give the lowest value of reduced chi-square (χ^2_{red}).

Modeled ^{210}Po profiles (Figure 1 and Table S1) calculated from measured ^{210}Pb values matched measured ^{210}Po profiles, with higher values being seen at the surface and at 1000 m, and the highest disequilibrium being observed between 50 and 100 m (Figure 1). The Pearson's chi-squared test indicated a good fit for all profiles, with χ^2_{red} ranging from 0.66 ($n = 11$) to 3.73 ($n = 13$), where n is the total number of depths (Table 2).

The lowest offsets between modeled and observed values are found between 200 and 800 m (9% averaged standard deviation, Table S1). The worst fits were found at 800–1000 m, where observations were lower than predicted by the model. Measured ^{210}Po and ^{210}Pb do not reach secular equilibrium; for instance, the difference at St. 16477 was as high as 35%. This contrasts with the predictions of the model, which suggests close activities for ^{210}Po and ^{210}Pb at 1000 m in all the profiles. We believe that this is caused by the model incorrectly assuming a constant value of δ below the euphotic zone. If we allow δ to increase by 25% at 800 m in the model, then modeled and measured ^{210}Po agree well. The reasons for the ^{210}Po-^{210}Pb disequilibrium found below 1000 m are not yet well determined [*Church et al.*, 2012]. According to the model presented here, secular equilibrium is broken below 1000 m when $\delta(x)$ increases. This increasing can be

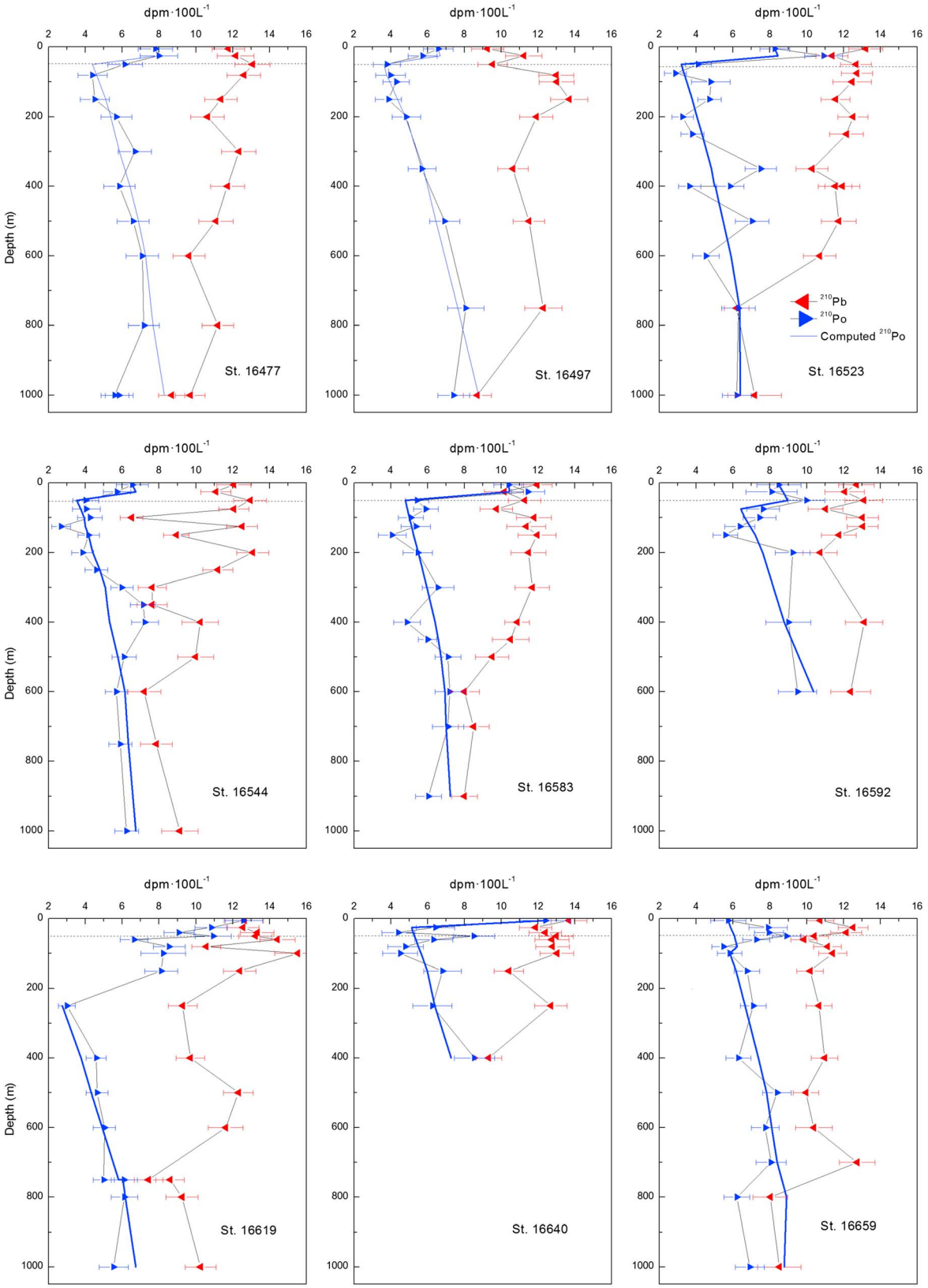

Figure 1. ^{210}Po and ^{210}Pb depth profiles measured in Porcupine Abyssal Plain (PAP) site during July 2009. Modeled data showing ^{210}Po from ^{210}Pb experimental data and using a one-box model. $\delta(z)$ is the parameter that needs to be tuned (see equations (5) and (6)) and is obtained by optimizing χ^2_{red} from calculated ^{210}Po and experimental ^{210}Po. Dash line corresponds to the mixed layer depth.

Table 2. $\delta(z)$ and χ^2_{red} Values of the ^{210}Po Fitting[a]

Station	χ^2	z(m)	$^{210}Po_{particles}$ (dpm·100 L^{-1})	±σ	f	±σ	δ(m)	v(m·d^{-1})	±σ
16477	*0.77*	50	0.48	0.04	0.079	0.014	610	70	10
		150	0.25	0.03	0.057	0.012	1130	100	20
		400	0.53	0.06	0.091	0.017	1130	65	10
16497	*0.37*	50	0.56	0.08	0.149	0.035	595	40	9
		150	0.40	0.05	0.103	0.023	1135	55	15
		500	0.53	0.06	0.076	0.012	1135	75	15
16523	*2.90*	50	0.73	0.05	0.179	0.033	595	45	9
		150	0.39	0.04	0.082	0.013	1605	100	15
		400	0.53	0.06	0.091	0.015	1605	90	15
16544	*1.87*	50	0.73	0.05	0.183	0.034	595	30	6
		150	0.39	0.04	0.093	0.015	1170	65	10
		400	0.53	0.06	0.073	0.011	1170	80	15
16583	*1.23*	50	0.30	0.03	0.056	0.009	600	115	20
		150	0.40	0.05	0.099	0.023	1310	65	15
		300	0.47	0.08	0.071	0.015	1310	95	20
		900	0.31	0.05	0.051	0.009	1310	150	30
16592	*1.96*	50	0.42	0.05	0.042	0.007	410	50	8
		150	0.32	0.04	0.058	0.009	590	50	9
		400	0.32	0.05	0.036	0.007	590	80	15
		600	0.35	0.07	0.037	0.008	590	80	20
16619	*1.04*	50	0.35	0.04	0.032	0.004	600	95	15
		150	0.41	0.04	0.050	0.007	1000	120	20
		400	0.32	0.05	0.071	0.013	1180	85	15
16640	*3.73*	50	0.27	0.03	0.032	0.006	1130	180	35
		150	0.16	0.02	0.023	0.005	1130	250	50
		400	0.32	0.05	0.038	0.007	1130	150	30
16659	*3.16*	50	0.94	0.06	0.106	0.012	820	40	5
		150	0.58	0.05	0.086	0.011	820	50	7
		400	0.32	0.05	0.051	0.009	895	95	15
Average from		**50**	**0.60**	**0.20**	**0.10**	**0.06**	**1023**	**60**	**30**
all stations		**150**	**0.40**	**0.10**	**0.080**	**0.02**	**1127**	**75**	**25**
		400–900	**0.40**	**0.10**	**0.065**	**0.02**	**1067**	**90**	**20**

[a] $\delta(z)$ is the tuned parameter of the model that optimizes χ^2_{red}. $^{210}Po_{particles}$ (dpm·100 L^{-1}) correspond to specific ^{210}Po activity measured in particles collected from in situ pumps filters (particles size >1 and >1–53 μm). *f* is the specific ^{210}Po activity in particulate fraction (particles size >1 μm) to total activity. *v(z)* is the average particle settling speed obtained using modeled δ and measured *f*.

ascribed either to an increase in the particle sinking velocities (which will be further discussed in section 4.2) or to a change in the ratio of particulate ^{210}Po to total ^{210}Po (i.e., a change in the *f(x)* parameter). An increase in the particulate to total ^{210}Po ratio would be associated to a constant scavenging of ^{210}Po by the particles while they sink, in contrast to the scavenging of ^{234}Th where an equilibrium of ^{234}Th in the particulate-dissolved phases is reached. This is supported by the fact that ^{234}Th-^{238}U reach equilibrium at shallow depth (200 m), whereas ^{210}Po-^{210}Pb never reach equilibrium before 500 m [*Bacon et al.*, 1976; *Hong et al.*, 2013; *Verdeny et al.*, 2008].

3.4. Sinking Speeds

Mean settling speeds diagnosed from the model at 50, 150, and 400–600 m (labeled as 500 m) using data from nine stations are shown in Figure 2 and Table 3. At 50 m, average sinking speeds show high scatter with a standard deviation of 50%. The scatter decreases to a standard deviation of 25% at 150 m and 20% at 500 m. Despite the spread in data, an increase in velocity with depth is observed. Average values increased from 60 ± 30 m·d^{-1} at 50 m to 75 ± 25 m·d^{-1} and 90 ± 20 m·d^{-1}, at 150 and 500 m, respectively, with a correlation between sinking speed and depth occurring ($p = 0.002$, $R = 0.58$, $n = 27$).

3.5. Application to ^{234}Th and Sensitivity Analysis

Similar reasoning to that outlined above regarding the interpretation of ^{210}Po-^{210}Pb profiles can be applied to the analogous radioactive pair of ^{234}Th-^{238}U, which was also measured alongside our ^{210}Po-^{210}Pb

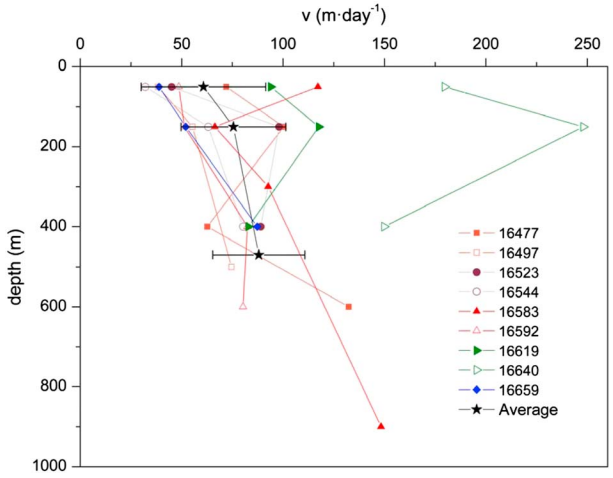

Figure 2. Average particle settling speeds ($m \cdot d^{-1}$) calculated at the PAP site during July 2009 for nine stations (uncertainties are given in Table 2). Average value for 50, 150, and 500 m depths are obtained. Uncertainty bars of the average values correspond to one standard deviation.

measurements. Details of collection, measurement, and results of ^{234}Th specific activities at the PAP site are found in *Le Moigne et al.* [2013b], where POC-Th and POC-Po derived fluxes were presented. Sinking rates from ^{234}Th results are shown in Table 3 (supplementary information in Table S2). ^{234}Th and ^{238}U modeled and measured profiles are presented in Figure S4. The differences between modeled and measured values range from 1 to 15%.

As the half-life of ^{234}Th is only 24 days, equilibrium with ^{238}U is found at around 150–200 m, which is shallower than the depth at which the ^{210}Po-^{210}Pb pair reaches equilibrium. Average velocities can therefore only be obtained at 50 and 150 m (Table 3). An increase in speed with depth is clearly observed at all stations with average velocities rising from $70 \pm 20\ m \cdot d^{-1}$ at 50 m to $130 \pm 20\ m \cdot d^{-1}$ at 150 m. These are slightly higher but similar to the velocities obtained from the Po-Pb profiles. An analogous correlation between sinking speed and depth is observed ($p = 0.00004$, $R = 0.8$, $n = 22$). However, low resolution of the ^{234}Th profiles collected during D341 (Table S2) prevents the full potential ability of the inverse model to extract sinking velocities from ^{234}Th measurements to be explored here. If this method is to be used systematically with ^{234}Th data to derive sinking velocities we recommend that high resolution ^{234}Th profiles be taken from surface to 150–200 m, the depth at which ^{238}U and ^{234}Th are likely to reach secular equilibrium.

Table 3. $\delta(z)$ and χ^2_{red} Values of the ^{234}Th Fitting[a]

Station	*z(m)*	$^{234}Th_{particles}$ *(dpm·100 L^{-1})*	±σ	*f*	±σ	*δ(m)*	*v(m·d^{-1})*	±σ
16477	50	0.050	0.006	0.024	0.006	70	82	31
	150	0.038	0.004	0.016	0.003	70	127	33
16497	50	0.058	0.006	0.021	0.004	350	97	24
	150	0.035	0.004	0.013	0.002	350	153	36
16523	50	0.056	0.004	0.028	0.003	45	71	10
	150	0.041	0.004	0.014	0.002	45	140	23
16544	50	0.056	0.006	0.027	0.003	45	76	13
	150	0.041	0.004	0.017	0.002	45	118	22
16559	50	0.056	0.006	0.023	0.003	30	86	14
	150	0.041	0.004	0.017	0.002	30	121	19
16583	50	0.079	0.009	0.032	0.004	30	62	11
	150	0.046	0.005	0.018	0.002	30	112	19
16592	50	0.066	0.007	0.044	0.005	40	46	8
	150	0.031	0.003	0.013	0.002	40	153	25
16619	50	0.072	0.008	0.031	0.004	20	64	13
	150	0.063	0.007	0.025	0.003	20	80	14
16640	50	0.048	0.005	0.019	0.002	15	105	18
	150	0.036	0.004	0.014	0.002	15	140	22
16659	50	0.092	0.011	0.058	0.008	35	35	7
	150	0.041	0.027	0.016	0.002	35	122	23
Average from all stations	**50**	**0.065**	**0.015**	**0.030**	**0.010**	**68**	**70**	**20**
	150	**0.04**	**0.01**	**0.015**	**0.003**	**68**	**130**	**20**

[a] $\delta(z)$ is the tuned parameter of the model that optimizes χ^2_{red}. $^{234}Th_{particles}$ *(dpm·100 L^{-1})* correspond to specific ^{234}Th activity measured in particles collected from in situ pumps filters (particles size >1 and >1–53 μm). *f* is the specific ^{234}Th activity in particulate fraction (particles size >1 μm) to total activity. $\delta(z)$ is the fitting parameter of the model that optimizes χ^2_{red}. The term *v(z)* is the average particle settling speed obtained using modeled δ and measured *f*.

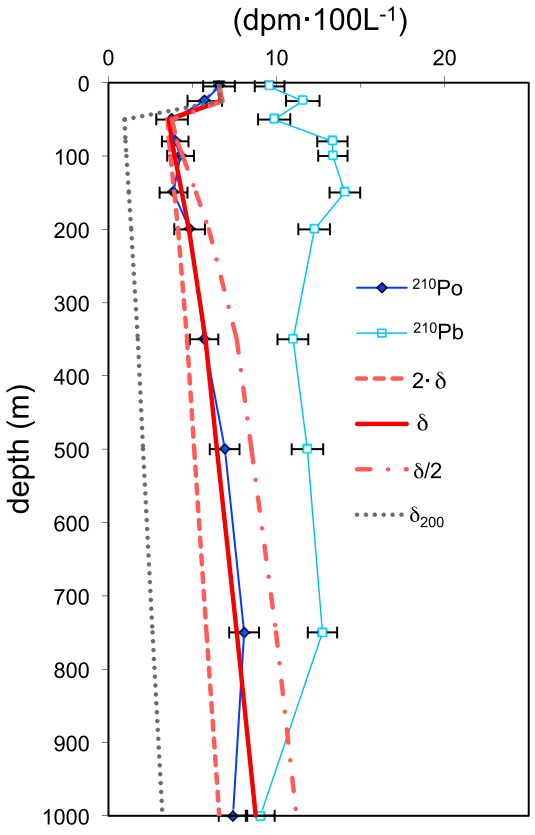

Figure 3. Specific ^{210}Po and ^{210}Pb activity profiles, Station 16977. ^{210}Po modeled profiles using: (i) optimized δ parameter, solid line; (ii) twice the optimized δ parameter, dashed line; (iii) half the optimized δ parameter, δ dotted-dashed line; and (iv) δ parameter for sinking speed $v = 200$ m/d, dotted line.

We undertook a sensitivity analysis in which the speed is doubled or halved (and δ changed accordingly) in a profile (e.g., St 16977) and the shape of the modeled speed profile examined (Figure 3). No significant changes are observed at shallower depths; however, halving δ (lower velocities according to Equation (10) produces lower ^{210}Po-^{210}Pb deficits at depth, and the ^{210}Po-^{210}Pb equilibrium is reached faster. Conversely, according to our model doubling δ (higher velocities) leads to a higher deficit at depth and equilibrium is reached at depths greater than 1000 m. This indicates that both the extent of the ^{210}Po-^{210}Pb disequilibrium and the depth at which secular equilibrium is reached are very sensitive to sinking velocities and can therefore be used to qualitatively determine sinking velocities in that area.

Finally, since it was previously suggested that in the northwest Mediterranean the main contributors to the flux from the euphotic to the twilight zone are predominantly fast (200 m·d^{-1}) and large (>70 μm) particles [*Abramson et al.*, 2010], we altered the sinking speed in our model to 200 m·d^{-1} (δ_{fast}), to test this hypothesis at the PAP site. The results, shown in Figure 3, do not compare well with the observations and no equilibrium is found at depth.

4. Discussion

4.1. Limitations of the Approach

The most widespread application of ^{210}Po-^{210}Pb (and ^{234}Th-^{238}U) depth profiles is to quantitatively estimate particle export (e.g., *Buesseler et al.* [2008]; *Le Moigne et al.* [2013a]; *Le Moigne et al.* [2013b]; *Verdeny et al.* [2009] and *Murray et al.* [2005]) rather than to derive sinking speeds. ^{210}Po (or ^{234}Th) export is calculated using an export model, and subsequently the downward flux is converted to POC (or PIC, trace metal, etc.) flux via a known tracer/Th ratio. The simplest export model combines particulate and dissolved polonium (or thorium) into a single box [*Savoye et al.*, 2006]. Two-box models differentiate between dissolved and particulate phases (e.g., *Bacon and Anderson* [1982] or *Friedrich and van der Loeff* [2002]), and more sophisticated models also discriminate between small and large fractions [e.g., *Marchal and Lam*, 2012].

The limitation of the one-box model is that it provides no information on removal processes such as adsorption, biological uptake, and colloidal interactions. In order to analyze such processes a more complex model is needed such as the three-box model described by *Marchal and Lam* [2012] which estimates the rate constants for ^{234}Th sorption onto large and small particles using inverse techniques. In contrast, instead of the rate constants we can estimate depth variation in settling rate, since in our model the rate constant is written in terms of speed and a tuning parameter

In most models that extract export data from radiotracer profiles a steady state (SS) model is used to estimate flux, while the more difficult to treat non-steady state (NNS) models are undertaken in situations where rapidly changing conditions render the steady state assumption invalid, such as bloom events [*Baena et al.*, 2008; *Buesseler et al.*, 1992; *Cochran et al.*, 2009]. The steady state assumption is less valid for ^{210}Po than for ^{234}Th due to its longer half-life [*Bacon et al.*, 1980; *Friedrich and van der Loeff*, 2002]. Nonetheless, most of the analyses undertaken for ^{210}Po assume steady state due to the inherent limitations of sampling strategies

during cruises (e.g., *Murray et al.* [2005]; *Stewart et al.* [2010] and *Verdeny et al.* [2008]): stations are normally sampled once while NSS equations can only be applied to ^{210}Po in stations sampled 2–3 months apart [*Stewart et al.*, 2007b].

Data from other authors obtained during the same cruise show that physical and biogeochemical conditions at the site were relatively constant during the course of this study. For instance, chlorophyll and PP data remained stable during the sampling period [*Le Moigne et al.*, 2013b]. In addition advection is believed to be moderate at the site [*Giering et al.*, 2014], T/S profiles show the presence of a single water mass (ENACWp) between the MLD and ~600 m at all stations (Figure S3), and current velocities were <5 m·d^{-1} [*Giering et al.*, 2014] with the MLD remaining relatively constant (range 31–62 m, Figure S2). Overall, the conditions during the cruise were relatively stationary, suggesting that steady state conditions prevailed over the 27 day sampling period and hence that the mean profile and the mean sinking speeds likely represent the average conditions at the site.

However, since D341 took place approximately 1 month after the bloom period [*Le Moigne et al.*, 2013b] there could be a temporal mismatch between the ^{210}Po-^{210}Pb deficit in the water column (which might be partially driven by the spring bloom) and the particulate ^{210}Po sampled during the post-bloom period [*Buesseler et al.*, 2006], a factor which may affect the SS assumption [*Cochran et al.*, 2009]. Particles collected during the cruise represent a blend of recently synthesized material and any particles which might have been created prior to the sampling period and then sunk slowly out of the mixed layer, e.g., fast particles created during the bloom period (>100 m·d^{-1}) would not be present in the water column sampled in July. However, particles from the bloom period sinking at 10 m·d^{-1} would still be present below the 300 m when the sampling cruise took place. Thus, v at the shallowest depths is likely to be driven by the prevailing post-bloom situation during the cruise, with deeper values being more influenced by any remnant slow-sinking particles which exited the bloom several weeks prior to sampling.

Any effect from the increase in production occurring during the bloom period will gradually decay with time until a steady state profile is reached, which will result in time-independent ^{210}Po fluxes over the course of the post-bloom period. Thus, in order to assess the validity of the steady state assumption one could simply compare ^{210}Pb-^{210}Po profiles sampled from the same location but at different times. Unfortunately, most of the locations where sampled only once during the cruise except for stations 16497 and 16619 which sampled the same location 18 days apart (Table 1). ^{210}Po fluxes at 16497 and 16619 stations were found to be significantly different from each other (65 ± 5 and 44 ± 5 dpm/m^2/d respectively at 150 m) [*Le Moigne et al.*, 2013b]. Since advection was shown to be low at the PAP site, the difference between fluxes and ^{210}Po measured activities at the two stations could be due to non-steady state effects. With this assumption we estimate the time derivative in equation (1) as being $da_{210_{Po}}(t)/dt = 0.013$ dpm·100 L^{-1} d^{-1}. When this value is included in equation (8) and the δ parameter is re-evaluated the changes in δ are $<10\%$. We therefore conclude that the site was close enough to SS conditions for the purpose of this study and that the systematic error in estimating sinking speeds introduced by the steady state assumption is smaller than the error in sinking velocity quantified by the range observed from the various stations.

A final possible source of error is that large particles may be under-sampled due to the inlet design of the SAPS and to the methodology used to wash them off the 53 μm mesh [*Liu et al.*, 2009]. If particulate ^{210}Po were underestimated, then the sinking velocities from equation (6) would be overestimated, leading to a higher contribution of slow-sinking particles to flux.

One of the motivations of this study is to analyze the extent to which the simplest export model (one-box, steady state) can reproduce measured ^{210}Po profiles. The good agreement between modeled and observed specific ^{210}Po activities (Figure 1 and Table 2) and between ^{234}Th and ^{210}Po derived results (Tables 2 and 3) suggests that the single box steady state model is an appropriate tool for interpreting data in this region during the study period, where the biogeochemical and physical conditions remained relatively constant and where ^{210}Po profiles sampled 18 days apart showed average relative variations of less than 10%.

4.2. Sinking Speeds

4.2.1. Contribution of Slow-Sinking Particles to Flux and Changes in Sinking Speed With Depth

Minimum and maximum sinking velocities of 30 ± 6 (St. 16544) and 130 ± 25 m·d^{-1} (St. 16583) were found at 50 and 400 m, respectively, with average values increasing from 60 ± 30 m·d^{-1} at 50 m to 90 ± 20 m·d^{-1} at 500 m. These values are significantly below 150–200 m·d^{-1}, the reported average values for fast-sinking

particles [*Turner*, 2002]. ^{234}Th derived sinking velocities are 70 ± 20 m·d^{-1} at 50 m and 130 ± 20 m·d^{-1} at 150 m. Furthermore, our sensitivity analysis suggests that simulating the ^{210}Po profile using a sinking velocity of 200 m·d^{-1} in the model produces results inconsistent with the experimental data (Figure 3). We interpret these results as suggesting that either most particles are sinking at speeds which are not seen in the IRS synthesis of *Alonso-Gonzalez et al.* [2010], or more likely, that a significant fraction of the flux at the PAP site is carried by very slow-sinking particles, consistent with the suggestion of *Alonso-Gonzalez et al.* [2010].

Our estimates of bulk particle sinking speeds are lower than directly measured aggregate (0.2–0.5 mm^3) sinking speeds made at 50 m during the cruise [*Riley et al.*, 2012] which averaged 180 m·d^{-1}. However, *Riley et al.* [2012] also observed that 63 ± 12% of the sinking POC was driven by slow settling (~9 m·d^{-1}) particles, with the remaining 40% made up of the fast settling aggregates. If we combine these relative fractions and their sinking rates (181 and 9 m·d^{-1}, respectively), we arrive at an estimated settling velocity of 70 m·d^{-1} at 50 m. This bulk estimate is remarkably similar to our estimate of 60 ± 30 m·d^{-1} at 50 m.

It is unclear how deep the slow-sinking particles penetrate into the mesopelagic, although *Riley et al.* [2012] hypothesize that most of these particles will be lost in the upper water column, with the deep flux being driven by remaining fast-sinking aggregates. Our average sinking speeds of 75 m·d^{-1} at 150 m, and 90 m·d^{-1} at 500 m are considerably slower than the sinking speeds of the aggregates measured by *Riley et al.* [2012] suggesting that either slow-sinking particles contribute to flux deep into the twilight zone or that the sinking speeds of aggregates decline significantly in the upper mesopelagic.

In equation (3), ^{210}Po flux can increase with depth due to either (i) an increase in the ^{210}Po transported by sinking particles (e.g., due to a creation of particles in the euphotic zone or to the accumulation of ^{210}Po in extant particles) or (ii) to an increase in sinking speed with depth. The increase in ^{210}Po flux between 0 and 1000 m is probably a combination of both factors.

We observe a moderate positive correlation between sinking velocities and depth ($p = 0.002$, $R = 0.58$, $n = 27$ using ^{210}Po and $p > 0.001$, $R = 0.80$, $n = 22$ using ^{234}Th) with average sinking velocities increasing from 50 m (60 m·d^{-1}) to 150 m (75 m·d^{-1}) and 500 m (90 m·d^{-1}). These data provide evidence for a moderate increase in bulk sinking velocity below the euphotic zone. We also found a positive correlation between depth and sinking speed ($p < 0.001$, $R = 0.611$, $n = 32$) in the Irminger and Iceland Basins during the July 2010) using the model presented here [*Villa-Alfageme et al.*, 2013].

4.2.2. Comparison With Previous Work

The presence of relatively slow-sinking material (<10 m·d^{-1}) at depth was also documented in the VERTIGO campaigns at K2 and ALOHA sites by *Trull et al.* [2008] using IRS traps. IRS sediment traps at 260 m [*Alonso-Gonzalez et al.*, 2010] suggest that slowly sinking material makes substantial contributions to deep flux in the Canary Current (Central Atlantic) under some circumstances. During summer and fall 60% of total POC flux was in the slowest settling class (0.7–11 m·d^{-1}) with 25% of the POC being carried by fast-sinking particles sinking at >320 m·d^{-1}. If these are weighted by their corresponding contributions to the flux then an average speed of 107 m·d^{-1} is found, similar to our estimate of velocity at 500 m.

Larger contributions of the slow-sinking particles to flux have been identified in the subtropical gyre at ALOHA (subtropical) than in the subarctic at K2 [*Trull et al.*, 2008] due to differences in ballasting and zooplankton pellet size [*Buesseler et al.*, 2007]. In the North Atlantic the contribution of slow-sinking particles to flux at the PAP site is comparable to the contributions at ALOHA and at the Canary Islands despite the differences in the ecosystems involved, suggesting that the pattern we observe is rather widespread. It is worth noticing that the size and speed of sinking particles vary in space and time. Thus, subtropical oligotrophic ecosystems are dominated by picophytoplankton and export is often driven by aggregates of small cells and rarely by large, rapidly sinking individual cells [*Stewart et al.*, 2010]. This diverges from the community in a subarctic ecosystem such as K2, with high nutrient conditions and higher production and export and where a large fraction (15–45%) of the flux was contributed by fast-sinking classes (410–205 m·d^{-1}) [*Trull et al.*, 2008]. Also, the seasonality is a decisive parameter, since larger and faster organisms appear during the first stages of the bloom but when the productive season advances the community shifts to smaller and slower phytoplankton species.

Overall both the IRS trap data summarized by *Alonso-Gonzalez et al.* [2010] and the radiotracer data reported here indicate that slow-sinking particles on occasion make significant contributions toward flux beneath

the euphotic zone. Open questions include how significant this flux is, how deep it penetrates, and what regulates its presence. The interpretation of ^{210}Po-^{210}Pb profiles presented here would, if applied globally to a large enough dataset allow these questions to be addressed.

4.3. Implications for Our Understanding of Particle Dynamics

An increase in sinking speed with depth can occur either due to (i) a change in particle characteristics during export [e.g., *Fowler and Knauer* [1986]] or to (ii) the gradual elimination of the slow-sinking fraction, as suggested by *Riley et al.* [2012].

According to Stokes' Law, particle velocities can increase as they sink due to either an increase in size or to an increase in density or to both effects simultaneously [*Armstrong et al.*, 2009]. Both changes might be associated with radiolarian populations at PAP site that contributed to the abnormally large POC flux observed during 2001 [*Lampitt et al.*, 2009]. According to *Riley et al.* [2012] radiolaria may have acted as nucleation points for detrital material, incorporating it into fast-sinking aggregates termed Aggregate Protist Complexes. In addition the production of sticky transparent exopolymer particles (TEP) [*De La Rocha and Passow*, 2007] by diatoms might contribute to the formation of fast-sinking aggregates.

The combination of our results with those of *Riley et al.* [2012] and *Alonso-Gonzalez et al.* [2010] suggests that there may be a significant contribution of slow-sinking ($<10\,m\cdot d^{-1}$) particles to the flux at shallow (50 m) and mesopelagic (150–400 m) depths. The slow-sinking particles in the mesopelagic could originate from either (a) the slow-sinking material found at shallow depths sinking deeper into the water column or (b) to slowly sinking particles formed at depth by aggregation and disaggregation processes, by microbial activity or by the self-assembly of dissolved organic material [*Alonso-Gonzalez et al.*, 2010; *Maiti et al.*, 2010; *Trull et al.*, 2008].

Option (b) is supported by *Giering et al.* [2014] who analyzed carbon demand and remineralization processes at the PAP site during D341. Their major conclusion was that the key role of mesopelagic zooplankton is to degrade large (fast) sinking particles into smaller (slow) particles which are subsequently remineralized by microbes. The slow-sinking particles that we suggest occur below the euphotic zone are likely to be created this way.

Regardless of their origin, slow-sinking particles are likely to be preferentially remineralized compared to fast-sinking material *[Abramson et al.,* 2010; *Buesseler et al.,* 2007; *Trull et al.,* 2008] due to their longer residence times at any particular depth. Their likely fate, rather than sinking, is ingestion and respiration by zooplankton and bacteria [*Trull et al.*, 2008]. Furthermore, interior respiration is dominated by prokaryotic bacteria rather than zooplankton at the PAP site [*Giering et al.*, 2014].

Boyd and Trull [2007] suggested that the power law expression that describes particle flux attenuation can be explained not only by the inherent decrease of particle degradation rates with depth but also by a downward increase of sinking rates. The balance of these two effects is hard to establish as most measurement methodologies probe fast-sinking particles preferentially [*Berelson*, 2002; *Pilskaln et al.*, 1998].

Our work suggests that a downward increase in average speeds plays some part in creating the power law relationship observed, as slow-sinking particles are remineralized in the twilight zone with fast particles dominating the flux at 1000 m as suggested by *Armstrong et al.* [2009]. Alternatively or additionally the velocities of the large fast-sinking particles may themselves increase due to repackaging or remineralization [*Boyd and Trull*, 2007]. Our estimates of velocity at 500 m are lower than the fast-sinking particles observed by *Riley et al*. [2012], suggesting that this possibility cannot be excluded. Furthermore, we propose that at the PAP site the pool of slowly sinking particle is lost in the upper mesopelagic likely due to consumption by prokaryotes, as previously postulated by *Giering et al.* [2014]. A previous lack of accounting for slowly sinking particles in twilight zone carbon budgets may be a partial cause of the imbalance between supply and consumption of organic carbon in the mesopelagic, as discussed by *Burd et al.* [2010].

Our work cannot draw conclusions on the mechanisms of remineralization or repackaging which produce the sinking velocities diagnosed here. Further studies are therefore needed to determine the origin of the slow-sinking flux, its fate in the twilight zone in different biogeochemical settings, and its potential contribution toward understanding carbon budgets. *Bopp et al.* [2005] predicted future shifts from biomineralizing species such as diatoms toward smaller (more slowly sinking) species due to future changes in ocean stratification and associated reductions in nutrient supply. We therefore consider it of major

importance to ascertain the role of small particles throughout the water column in order to determine whether such a shift might change the efficiency of POC transport to depth.

5. Conclusions

The ^{210}Po-^{210}Pb deficit in the water column is used to estimate the depth dependency of particle settling speed. Sensitivity tests show that the ^{210}Po deficit below the euphotic zone cannot be exclusively due to fast particles sinking with velocities close to 200 m s^{-1}. A moderate depth dependency in settling speed was found with average speeds of 60 ± 30 m·d^{-1} at 50 m, 75 ± 25 m·d^{-1} at 150 m and 90 ± 20 m·d^{-1} at 500 m. Similar results have been found for ^{234}Th-derived sinking activities. This approach yields sinking velocities similar to those obtained by *Riley et al.* [2012] from the same cruise and confirms that there might be a contribution of slow-sinking particles to the carbon flux below the euphotic zone. Our results may have implications for closing mesopelagic carbon budgets and suggest that ascertaining sinking velocities is significant for the prediction of biological carbon storage in an ocean whose population is predicted to shift toward small phytoplankton at the expense of diatoms.

Acknowledgments
We would like to thank the captain and crew of the RRS Discovery and the D341 scientific team. This work was partly supported by Junta de Andalucía, project P07-RNM-02567, Spain (MVA), by the CalMarO FP7 Marie Curie initial training network (FLM) and by the U.K. Ocean 2025 program (RS). Data are held at the British Oceanographic Data Centre (http://www.bodc.ac.uk).

References

Abramson, L., C. Lee, Z. F. Liu, S. G. Wakeham, and J. Szlosek (2010), Exchange between suspended and sinking particles in the northwest Mediterranean as inferred from the organic composition of in situ pump and sediment trap samples, *Limnol. Oceanogr.*, *55*(2), 725–739.

Alldredge, A. L., and C. C. Gotschalk (1989), Direct observations of the mass flocculation of diatom blooms - Characteristics, settling velocities and formation of diatom aggregates, *Deep-Sea Res.*, *36*(2), 159–171.

Alonso-Gonzalez, I. J., J. Aristegui, C. Lee, A. Sanchez-Vidal, A. Calafat, J. Fabres, P. Sangra, P. Masque, A. Hernandez-Guerra, and V. Benitez-Barrios (2010), Role of slowly settling particles in the ocean carbon cycle, *Geophys. Res. Lett.*, *37*, L13608, doi:10.1029/2010GL043827.

Armstrong, R. A., M. L. Peterson, C. Lee, and S. G. Wakeham (2009), Settling velocity spectra and the ballast ratio hypothesis, *Deep Sea Res. Part II*, *56*(18), 1470–1478.

Bacon, M. P., and R. F. Anderson (1982), Distribution of thorium isotopes between dissolved and particulate forms in the deep-sea, *J. Geophys. Res.*, *87*(Nc3), 2045–2056, doi:10.1029/JC087iC03p02045.

Bacon, M. P., D. W. Spencer, and P. G. Brewer (1976), Pb-210-Ra-226 and Po-210-Pb-210 disequilibria in seawater and suspended particulate matter, *Earth Planet. Sci. Lett.*, *32*(2), 277–296.

Bacon, M. P., P. G. Brewer, D. W. Spencer, J. W. Murray, and J. Goddard (1980), Pb-210, Po-210, Manganese and Iron in the Cariaco Trench, *Deep-Sea Res.*, *27*(2), 119–135.

Baena, A. M. R. Y., R. Boudjenoun, S. W. Fowler, J. C. Miquel, P. Masque, J. A. Sanchez-Cabeza, and M. Warnau (2008), Th-234-based carbon export during an ice-edge bloom: Sea-ice algae as a likely bias in data interpretation, *Earth Planet. Sci. Lett.*, *269*(3–4), 595–603.

Berelson, W. M. (2002), Particle settling rates increase with depth in the ocean, *Deep Sea Res. Part II*, *49*(1–3), 237–251.

Bopp, L., O. Aumont, P. Cadule, S. Alvain, and M. Gehlen (2005), Response of diatoms distribution to global warming and potential implications: A global model study, *Geophys. Res. Lett.*, *32*, L19606, doi:10.1029/2005GL023653.

Boyd, P. W., and T. W. Trull (2007), Understanding the export of biogenic particles in oceanic waters: Is there consensus?, *Prog. Oceanogr.*, *72*(4), 276–312.

Buesseler, K. O., M. P. Bacon, J. K. Cochran, and H. D. Livingston (1992), Carbon and nitrogen export during the JGOFS North Atlantic Bloom Experiment estimated from ^{234}Th:^{238}U disequilibria, *Deep Sea Res. Part I*, *39*(7–8), 1115–1137.

Buesseler, K. O., L. Ball, J. Andrews, J. K. Cochran, D. J. Hirschberg, M. P. Bacon, A. Fleer, and M. Brzezinski (2001), Upper ocean export of particulate organic carbon and biogenic silica in the Southern Ocean along 170 degrees W, *Deep Sea Res. Part II*, *48*(19–20), 4275–4297.

Buesseler, K. O., et al. (2006), An assessment of particulate organic carbon to thorium-234 ratios in the ocean and their impact on the application of (234)Th as a POC flux proxy, *Mar. Chem.*, *100*(3–4), 213–233.

Buesseler, K. O., et al. (2007), Revisiting carbon flux through the ocean's twilight zone, *Science*, *316*(5824), 567–570.

Buesseler, K. O., C. Lamborg, P. Cai, R. Escoube, R. Johnson, S. Pike, P. Masque, D. McGillicuddy, and E. Verdeny (2008), Particle fluxes associated with mesoscale eddies in the Sargasso Sea, *Deep Sea Res. Part II*, *55*(10–13), 1426–1444.

Burd, A., et al. (2010), Assessing the apparent imbalance between geochemical and biochemical indicators of meso and bathypelagic biological activity: What the @$#! is wrong with present calculations of carbon budgets?, *Deep Sea Res. Part II*, *57*, 1557–1571.

Burd, A. B., S. B. Moran, and G. A. Jackson (2000), A coupled adsorption-aggregation model of the POC/Th-234 ratio of marine particles, *Deep Sea Res. Part I*, *47*(1), 103–120.

Church, T., et al. (2012), Intercalibration studies of ^{210}Po and ^{210}Pb in dissolved and particulate seawater samples, *Limnol. Oceanogr. Meth.*, *10*, 776–789.

Cochran, J. K., and P. Masque (2003), Short-lived U/Th series radionuclides in the ocean: Tracers for scavenging rates, export fluxes and particle dynamics, *Rev. Mineral. Geochem.*, *52*, 461–492.

Cochran, J. K., et al. (2009), Time-series measurements of (234)Th in water column and sediment trap samples from the northwestern Mediterranean Sea, *Deep Sea Res. Part II*, *56*(18), 1487–1501.

De La Rocha, C. L. (2003), The biological pump, in *Treatise on Geochemistry*, edited by H. D. Holland and K. K. Turekian, pp. 1–29, Elsevier, Oxford, U. K.

De La Rocha, C. L., and U. Passow (2007), Factors influencing the sinking of POC and the efficiency of the biological carbon pump, *Deep Sea Res. Part II*, *54*(5–7), 639–658.

Falkowski, P. G., R. T. Barber, and V. Smetacek (1998), Biogeochemical controls and feedbacks on ocean primary production, *Science*, *281*(5374), 200–206.

Fisher, N. S., K. A. Burns, R. D. Cherry, and M. Heyraud (1983), Accumulation and cellular-distribution of ^{241}Am, ^{210}Po, and ^{210}Pb in two marine-algae, *Mar. Ecol. Prog. Ser.*, *11*(3), 233–237.

Fowler, S. W., and G. A. Knauer (1986), Role of large particles in the transport of elements and organic-compounds through the oceanic water column, *Prog. Oceanogr.*, *16*(3), 147–194.

Friedrich, J., and M. M. R. van der Loeff (2002), A two-tracer (^{210}Po–^{234}Th) approach to distinguish organic carbon and biogenic silica export flux in the Antarctic Circumpolar Current, *Deep Sea Res. I*, *49*(1), 101–120.

GEOTRACES Standards and Intercalibration Committee (Ed.) (2010), Sampling and Sample-handling Protocols for GEOTRACES Cruises, Geotraces.

Giering, S. L. C., et al. (2014), Reconciliation of the carbon budget in the ocean's twilight zone, *Nature*, *507*, 480–483.

Hartman, S. E., K. E. Larkin, R. S. Lampitt, M. Lankhorst, and D. J. Hydes (2010), Seasonal and inter-annual biogeochemical variations in the Porcupine Abyssal Plain 2003–2005 associated with winter mixing and surface circulation, *Deep Sea Res. Part II Top. Stud. Oceanogr.*, *57*(15), 1303–1312.

Henson, S., J. J. Dunne, and J. Sarmiento (2009), Decadal variability in North Atlantic phytoplankton blooms, *J. Geophys. Res.*, *114*, C04013, doi:10.1029/2008JC005139.

Henson, S. A., R. Sanders, and E. Madsen (2012), Global patterns in efficiency of particulate organic carbon export and transfer to the deep ocean, *Global Biogeochem. Cycles*, *26*, GB1028, doi:10.1029/2011GB004099.

Hong, G. H., M. Baskaran, T. M. Church, and M. H. Conte (2013), Scavenging, cycling and removal fluxes of ^{210}Po and ^{210}Pb at the Bermuda time-series study site, *Deep Sea Res. Part II Top. Stud. Oceanogr.*, *93*, 108–118.

Kwon, E. Y., F. Primeau, and J. L. Sarmiento (2009), The impact of remineralization depth on the air-sea carbon balance, *Nat. Geosci.*, *2*(9), 630–635.

Lampitt, R. S., I. Salter, and D. Johns (2009), Radiolaria: Major exporters of organic carbon to the deep ocean, *Global Biogeochem. Cycles*, *23*, GB1010, doi:10.1029/2008GB003221.

Lampitt, R. S., I. Salter, B. A. de Cuevas, S. Hartman, K. E. Larkin, and C. A. Pebody (2010), Long-term variability of downward particle flux in the deep northeast Atlantic: Causes and trends, *Deep Sea Res. Part II*, *57*(15), 1346–1361.

Le Moigne, F. A. C., S. A. Henson, R. J. Sanders, and E. Madsen (2013a), Global database of surface ocean particulate organic carbon export fluxes diagnosed from the ^{234}Th technique, *Earth Syst. Sci. Data*, *5*, 295–304.

Le Moigne, F. A. C., M. Villa, R. J. Sanders, C. Marsay, S. R. Henson, and R. García-Tenorio (2013b), Export of organic carbon and biominerals derived from ^{234}Th and ^{210}Po at the Porcupine Abyssal Plain, *Deep Sea Res. Part I*, *72*, 88–101.

Lee, C., M. L. Peterson, S. G. Wakeham, R. A. Armstrong, J. K. Cochran, J. C. Miquel, S. W. Fowler, D. Hirschberg, A. Beck, and J. H. Xue (2009), Particulate organic matter and ballast fluxes measured using time-series and settling velocity sediment traps in the northwestern Mediterranean Sea, *Deep Sea Res. Part II*, *56*(18), 1420–1436.

Liu, Z. F., J. K. Cochran, C. Lee, B. Gasser, J. C. Miquel, and S. G. Wakeham (2009), Further investigations on why POC concentrations differ in samples collected by Niskin bottle and in situ pump, *Deep Sea Res. Part II*, *56*(18), 1558–1567.

Maiti, K., C. R. Benitez-Nelson, and K. O. Buesseler (2010), Insights into particle formation and remineralization using the short-lived radionuclide, Thoruim-234, *Geophys. Res. Lett.*, *37*, L15608, doi:10.1029/2010GL044063.

Marchal, O., and P. J. Lam (2012), What can paired measurements of Th isotope activity and particle concentration tell us about particle cycling in the ocean?, *Geochim. Cosmochim. Acta*, *90*, 126–148.

McDonnell, A. M. P., and K. O. Buesseler (2010), Variability in the average sinking velocity of marine particles, *Limnol. Oceanogr.*, *55*(5), 2085–2096.

Murnane, R. J., and J. K. Cochran (1991), Particle cycling rate constants from nutrient particle and thorium isotope data in the Nw Atlantic-Ocean, in *Radionuclides in the Study of Marine Processes*, pp. 374, Springer, Netherlands.

Murnane, R. J., J. K. Cochran, and J. L. Sarmiento (1994), Estimates of particle-cycling and thorium-cycling rates in the Northwest Atlantic-Ocean, *J. Geophys. Res.*, *99*(C2), 3373–3392, doi:10.1029/93JC02378.

Murnane, R. J., J. K. Cochran, K. O. Buesseler, and M. P. Bacon (1996), Least-squares estimates of thorium, particle, and nutrient cycling rate constants from the JGOFS north Atlantic bloom experiment, *Deep Sea Res. Part I*, *43*(2), 239–258.

Murray, J. W., B. Paul, J. P. Dunne, and T. Chapin (2005), ^{234}Th, ^{210}Pb, ^{210}Po and stable Pb in the central equatorial Pacific: Tracers for particle cycling, *Deep Sea Res. Part I*, *52*(11), 2109–2139.

Peterson, M. L., P. J. Hernes, D. S. Thoreson, J. I. Hedges, C. Lee, and S. G. Wakeham (1993), Field-Evaluation of a Valved Sediment Trap, *Limnol. Oceanogr.*, *38*(8), 1741–1761.

Peterson, M. L., S. G. Wakeham, C. Lee, M. A. Askea, and J. C. Miquel (2005), Novel techniques for collection of sinking particles in the ocean and determining their settling rates, *Limnol. Oceanogr. Meth.*, *3*, 520–532.

Peterson, M. L., J. Fabres, S. G. Wakeham, C. Lee, I. J. Alonso, and J. C. Miquel (2009), Sampling the vertical particle flux in the upper water column using a large diameter free-drifting NetTrap adapted to an Indented Rotating Sphere sediment trap, *Deep Sea Res. Part II*, *56*(18), 1547–1557.

Pilskaln, C. H., C. Lehmann, J. B. Paduan, and M. W. Silver (1998), Spatial and temporal dynamics in marine aggregate abundance, sinking rate and flux: Monterey Bay, central California, *Deep Sea Res. Part II*, *45*(8–9), 1803–1837.

Resplandy, L., A. P. Martin, F. Le Moigne, P. Martin, A. Aquilina, L. Memery, M. Levy, and R. Sanders (2012), How does dynamical spatial variability impact ^{234}Th-derived estimates of organic export?, *Deep Sea Res. Part I*, *68*, 24–45.

Rigaud, S., V. Puigcorbé, P. Camara-Mor, N. Casacuberta, M. Roca-Martí, J. Garcia-Orellana, C. R. Benitez-Nelson, P. Masque, and T. Church (2013), An assessment of the methods, calculation and uncertainties in the determination of ^{210}Po and ^{210}Pb activities in seawater, *Limnol. Oceanogr. Meth.*, *11*, 561–571.

Riley, J., R. Sanders, C. Marsay, F. Le Moigne, E. Achterberg, and A. Poulton (2012), The relative contribution of fast and slow sinking particles to ocean carbon export, *Global Biogeochem. Cycles*, *26*, GB1026, doi:10.1029/2011GB004085.

Robinson, C., et al. (2010), Mesopelagic zone ecology and biogeochemistry – a synthesis, *Deep Sea Res. Part II*, *57*, 1504–1518.

Sanders, R., et al. (2014), The biological pump in the North Atlantic, *Prog. Oceanogr.* [Available at http://www.sciencedirect.com/science/article/pii/S0079661114000901.]

Savoye, N., C. Benitez-Nelson, A. B. Burd, J. K. Cochran, M. Charette, K. O. Buesseler, G. A. Jackson, M. Roy-Barman, S. Schmidt, and M. Elskens (2006), ^{234}Th sorption and export models in the water column: A review, *Mar. Chem.*, *100*(3–4), 234–249.

Smythe-Wright, D., S. Boswell, Y. N. Kim, and A. Kemp (2010), Spatio-temporal changes in the distribution of phytopigments and phytoplanktonic groups at the Porcupine Abyssal Plain (PAP) site, *Deep Sea Res. Part II*, *57*(15), 1324–1335.

Steinhoff, T., T. Friedrich, S. E. Hartman, A. Oschlies, D. W. R. Wallace, and A. Kortzinger (2010), Estimating mixed layer nitrate in the North Atlantic Ocean, *Biogeosciences*, *7*(3), 795–807.

Sternberg, R. W., I. Berhane, and A. S. Ogston (1999), Measurement of size and settling velocity of suspended aggregates on the northern California continental shelf, *Mar. Geol.*, *154*(1–4), 43–53.

Stewart, G., J. K. Cochran, J. H. Xue, C. Lee, S. G. Wakeham, R. A. Armstrong, P. Masque, and J. C. Miquel (2007a), Exploring the connection between Po-210 and organic matter in the northwestern Mediterranean, *Deep Sea Res. Part I*, *54*(3), 415–427.

Stewart, G., J. K. Cochran, J. C. Miquel, P. Masque, J. Szlosek, A. M. R. Y. Baena, S. W. Fowler, B. Gasser, and D. J. Hirschberg (2007b), Comparing POC export from ^{234}Th/^{238}U and ^{210}Po/^{210}Pb disequilibria with estimates from sediment traps in the northwest Mediterranean, *Deep Sea Res. Part I*, *54*(9), 1549–1570.

Stewart, G. M., S. B. Moran, and M. W. Lomas (2010), Seasonal POC fluxes at BATS estimated from ^{210}Po deficits, *Deep Sea Res. Part I*, *57*(1), 113–124.

Trull, T. W., S. G. Bray, K. O. Buesseler, C. H. Lamborg, S. Manganini, C. Moy, and J. Valdes (2008), In situ measurement of mesopelagic particle sinking rates and the control of carbon transfer to the ocean interior during the Vertical Flux in the Global Ocean (VERTIGO) voyages in the North Pacific, *Deep Sea Res. Part II*, *55*(14–15), 1684–1695.

Turner, J. T. (2002), Zooplankton fecal pellets, marine snow and sinking phytoplankton blooms, *Aquat. Microb. Ecol.*, *27*(1), 57–102.

Turner, J. T. (2014), Zooplankton fecal pellets, marine snow, phytodetritus and the ocean's biological pump, *Prog. Oceanogr.* [Available at http://www.sciencedirect.com/science/article/pii/S0079661114001281.]

Verdeny, E., P. Masque, K. Maiti, J. Garcia-Orellana, J. M. Brauch, C. Mahaffey, and C. R. Benitez-Nelson (2008), Particle export within cyclonic Hawaiian lee eddies derived from ^{210}Pb–^{210}Po disequilibrium, *Deep Sea Res. Part II*, *55*(10–13), 1461–1472.

Verdeny, E., P. Masque, J. Garcia-Orellana, C. Hanfland, J. K. Cochran, and G. M. Stewart (2009), POC export from ocean surface waters by means of ^{234}Th/^{238}U and ^{210}Po/^{210}Pb disequilibria: A review of the use of two radiotracer pairs, *Deep Sea Res. Part II*, *56*(18), 1502–1518.

Villa-Alfageme, M., F. de Soto, F. Le Moigne, S. Giering, R. Sanders, and R. Garcia-Tenorio (2013), Observations and modeling of sinking particle speeds in the twilight zone using ^{210}Po-^{210}Pb deficit, *Mineral. Mag.*, *77*(5), 2418.

Wilson, S. E., D. K. Steinberg, and K. O. Buesseler (2008), Changes in fecal pellet characteristics with depth as indicators of zooplankton repackaging of particles in the mesopelagic zone of the subtropical and subarctic North Pacific Ocean, *Deep Sea Res. Part II*, *55*(14–15), 1636–1647.

Xue, J. H., and R. A. Armstrong (2009), An improved "benchmark" method for estimating particle settling velocities from time-series sediment trap fluxes, *Deep Sea Res. Part II*, *56*(18), 1479–1486.